Article:
Sharma, S., Bose, A., Biswas, S. et al. (2025) Cyperus rotundus mediated green synthesis of silver nanoparticles for antibacterial wound dressing applications. Scientific Reports, 15. 18394. ISSN: 2045-2322

https://doi.org/10.1038/s41598-025-03555-x

scientific reports

Check for updates

OPEN

Cyperus rotundus mediated green synthesis of silver nanoparticles for antibacterial wound dressing applications

Susrita Sharma[1], Anindya Bose[1]✉, Soumojit Biswas[2], Shreeja Sen[1] & Ipsita Roy[2]

Wound healing is a complex biological process that can be hindered by persistent infections and inflammation, especially in the presence of multidrug-resistant (MDR) bacteria. Silver nanoparticles (AgNPs) have demonstrated significant antimicrobial efficacy; however, concerns regarding their toxicity have limited their therapeutic application. Methods: In this study, we developed a biocompatible Ag-NPs-based hydrogel using *Cyperus rotundus* extract via a green synthesis approach for prospective wound healing applications. The synthesized AgNPs were characterized for their physicochemical properties, confirming their stability and antibacterial potency against *E. coli* and *S. epidermidis*. The Ag-NPs-loaded hydrogel was formulated using Carbopol 974P and evaluated for its physicochemical properties, antibacterial activity, anti-inflammatory potential, and cytotoxicity. Results: Characterization studies confirmed the successful synthesis of AgNPs, exhibiting potent antibacterial, antioxidant, and anti-inflammatory properties. The Ag-NPs-loaded hydrogel demonstrated significant wound contraction in an excision wound model, comparable to standard treatment. Additionally, in vitro safety evaluations confirmed excellent biocompatibility, minimizing toxicity concerns associated with conventional silver formulations. Conclusions: These findings suggest that the developed Ag-NPs-based hydrogel is an effective, natural, and safer alternative for advanced wound care, warranting further clinical validation.

Keywords Wound healing, Silver nanoparticles, Antimicrobial resistance

A wound refers to any breakage to the epithelial tissue of the skin caused by cuts, scratches, accidents, or surgeries[1]. Though the human body's defence mechanism starts the repair naturally for damaged tissue, some major injuries take longer to heal. Additionally, such wounds may get infections, leading to persistent pain and inflammation[2]. The exposed wounded skin provides a conducive environment for microbial growth leading to colonization, aided by the secretion of an extracellular polymeric matrix, which protects the microbes from any outer defense mechanism like antibiotics[3].

Antibiotics can play a significant role in wound healing by preventing infections that impede repair. Antibiotic therapy is essential in infected wounds to manage conditions such as cellulitis, osteomyelitis, sepsis, lymphangitis, abscesses, and invasive tissue infections. However, inappropriate use of antibiotics may contribute to the emergence of antimicrobial resistance[4]. This presence of multidrug-resistant (MDR) bacterial strains adds a layer of complexity to wound management[5]. These antibiotic-resistant pathogens can significantly increase mortality and morbidity rates, extend recovery times, and escalate medical costs and treatment challenges, ultimately exacerbating the economic burden as the global wound care market, valued at $23.66 billion in 2023, is projected to reach $38.39 billion by 2034, reflecting a compound annual growth rate (CAGR) of 4.5% from 2024 to 2034[6].

As infection control is one of the matters of concern during the healing process, metals such as silver have become a good alternative to conventional antibiotics to treat skin infections. Silver treatments like silver nitrate and silver sulfadiazine act on the mechanism where the presented silver disrupts the cellular function of the microbes by blocking their respiratory enzyme activities. Silver can be rendered inactive by protein anions,

[1]School of Pharmaceutical Sciences, Siksha O Anusandhan (Deemed to be University), Bhubaneswar, Odisha 751003, India. [2]Department of Biotechnology, National Institute of Pharmaceutical Education and Research (NIPER), Sector 67, S.A.S. Nagar, S.A.S. Nagar, Punjab 160062, India. ✉email: anindyabose@soa.ac.in; anindyabose_in@yahoo.com

chloride ions, and bicarbonate present in body fluids. Moreover, prolonged use of silver can lead to cellular toxicity and, in some cases, may cause argyria (a blue-grey skin discoloration)[7].

The advancement of nanotechnology has significantly enhanced silver's efficacy as a potent antimicrobial agent. This improvement is attributed to its higher surface area-to-volume ratio and nanoscale size, which maximize interactions with various microorganisms. These silver nanoparticles actively combat the microbes by disrupting bacterial cell membranes, generating reactive oxygen species (ROS), leading to DNA damage and cellular dysfunction[8,9]. However, silver nanoparticles (Ag-NPs) can also present toxicity concerns for human cells. Research has shown that these nanoparticles can penetrate cell membranes and release silver ions, resulting in genotoxicity, cytotoxicity, and even cell death. Additionally, their high surface area and reactivity make Ag-NPs environmentally challenging, as their release into the environment complicates proper management and disposal[10].

Green synthesis of silver nanoparticles (AgNPs) using plant extracts has garnered significant attention due to its environmentally friendly approach and potential to reduce toxicity. Plant extracts act as natural reducing and capping agents, facilitating the formation of AgNPs without the need for harmful chemicals. This method not only minimizes environmental impact but also leverages the inherent biological activities of the plant compounds involved. For instance, the antioxidants present in plant extracts play a crucial role in reducing silver ions and stabilizing the nanoparticles, enhancing their biocompatibility and therapeutic potential[11]. Moreover, using plant extracts can improve the antibacterial properties of AgNPs, as the phytochemicals contribute additional antimicrobial effects[12]. This synergy between the plant-derived compounds and the silver nanoparticles not only enhances efficacy but also reduces the potential for adverse effects, making green-synthesized AgNPs a promising avenue for biomedical applications.

Cyperus rotundus, commonly known as nutgrass or Nagarmotha, is a perennial species from the Cyperaceae family, predominantly found in the tropical and subtropical regions of India. The plant is renowned for its rich phytochemical profile, which includes alkaloids, flavonoids, terpenoids, tannins, and other bioactive constituents that contribute to its wide-ranging pharmacological activities. These properties have cemented its role in both traditional and modern medicinal systems[13]. The rhizomes of the plant contain high levels of flavonoids, phenolics, alkaloids, and terpenoids, which serve as natural reducing and capping agents during nanoparticle synthesis. These compounds donate electrons to silver ions (Ag^+), facilitating the formation of silver nanoparticles[14]. These biomolecules not only mediate the formation of AgNPs but also impart antimicrobial, antioxidant, and anti-inflammatory properties, which are crucial in promoting wound healing and preventing infection.

This plant demonstrates significant antimicrobial properties, primarily due to its diverse range of phytochemicals, including sesquiterpenes, alkaloids, glycosides, and saponins. These compounds contribute to its ability to disrupt microbial cell membranes, inhibit essential microbial enzymes, interfere with nucleic acid functions, and induce apoptosis—mechanisms that collectively support effective wound healing through the elimination of pathogens[15]. In addition, *C. rotundus* has been found to enhance the antimicrobial activity of silver nanoparticles (AgNPs), promoting wound healing via synergistic effects[16]. Suman et al. (2013) successfully synthesized AgNPs using rhizome extracts of *C. rotundus*, reporting marked antibacterial effects against *Staphylococcus aureus* and *Pseudomonas aeruginosa*, attributed to the plant's phytochemical constituents[17]. Likewise, Sharma and Singh (2011) identified bioactive compounds—such as alkaloids, flavonoids, saponins, and tannins—in the rhizomes, reinforcing the plant's potent antimicrobial capacity. These findings underscore the potential of *C. rotundus* as a bioresource for producing therapeutically effective AgNPs[18].

Recognized for its extensive use in traditional medicine for treating skin ailments and promoting wound healing, *C. rotundus* possesses a diverse array of bioactive phytochemicals and notable pharmacological activities. These attributes position it as a valuable biological agent for the green synthesis of silver nanoparticles (AgNPs), offering a novel and efficacious platform for advanced wound care applications. Notably, a study conducted by Nagalakshmi et al. highlighted the wound healing potential of the plant's tuber extract, demonstrating significant wound contraction and accelerated closure rates[19].

Furthermore, *C. rotundus* is an invasive, widely available species that does not require specialized cultivation, making it a sustainable and low-cost resource, especially beneficial in resource-limited settings. Integrating its traditional medicinal use with modern nanotechnology not only adds value to an otherwise weedy species but also contributes to the development of effective, eco-friendly, and affordable wound care solutions.

This study aims to synthesize safe and biocompatible silver nanoparticles using Cyperus rotundus, with the goal of enhancing their antimicrobial activity and promoting wound healing through synergistic effects. The novelty of this approach lies in the strategic use of a medicinally valuable yet underutilized plant for nanoparticle synthesis, leveraging its dual role as both a green reducing agent and a natural source of wound-healing phytochemicals. This biogenic method not only aligns with the principles of green chemistry but also eliminates the need for toxic chemicals typically employed in conventional nanoparticle synthesis.

Hydrogel-based formulations have emerged as promising platforms in wound healing, owing to their unique physicochemical properties and versatile therapeutic benefits. One of their primary advantages lies in their ability to maintain a moist wound environment, which is crucial for accelerating tissue regeneration and minimizing scarring. Their high-water content not only provides a cooling and soothing effect on inflamed tissues but also enhances overall patient comfort. The porous, hydrophilic structure of hydrogels facilitates efficient gas exchange, supporting processes such as angiogenesis, while simultaneously acting as a physical barrier to microbial infiltration. Furthermore, their soft, flexible consistency allows for seamless application over uneven or complex wound surfaces, ensuring close contact and effective coverage[20,21]. In recent years, extensive research has focused on the use of both natural and synthetic polymer-based hydrogels for advanced wound care. These hydrogels not only provide a moist environment conducive to healing but also exhibit multifunctional therapeutic properties. One notable advancement is the bio-multifunctional hydrogel proposed by Yuanping et

al., composed of benzaldehyde-terminated 4-arm polyethylene glycol (4-arm-PEG-CHO) and carboxymethyl chitosan (CMCS), loaded with basic fibroblast growth factor (bFGF). This formulation significantly accelerated the healing of full-thickness diabetic wounds, demonstrating immense therapeutic potential[22]. Similarly, Lili et al. developed a biocompatible hydrogel using chitosan and dialdehyde bacterial cellulose, which exhibited excellent antibacterial activity, proper compressive properties, and desired water retention capacity. high biocompatibility, and strong wound healing efficacy[23]. These studies highlight the significant advantages of hydrogel-based systems as innovative platforms for advanced wound care, demonstrating their potential to enhance healing outcomes through moisture retention, biocompatibility, and controlled delivery of therapeutic agents.

Carbopol, renowned for its non-toxicity and excellent biocompatibility, offers superior water-retention capacity, which is vital for maintaining the moist environment necessary to accelerate tissue regeneration. Even at low concentrations, it forms a clear, stable gel with intrinsic bioadhesive qualities, ensuring prolonged adherence to the wound surface. Additionally, its cooling and soothing effects provide relief at the application site while further supporting tissue recovery[24]. In the present study, the synthesized nanoparticles were incorporated into a Carbopol-based hydrogel to develop an advanced nanosilver formulation. Carbopol was purposefully selected as the hydrogel matrix due to its exceptional physicochemical properties, which align well with the critical requirements for effective wound healing.

Experimental work

Materials

The dried rhizomes of *C. rotundus* were procured from the local market in Cuttack. Silver nitrate and Carbopol 974P were obtained from Sisco Research Laboratory (SRL), while triethanolamine was sourced from Pure Chemicals. Ethanol and distilled water were utilized for cleaning purposes. All chemicals used in this research were of analytical grade to ensure the accuracy and reliability of results.

Silver nanoparticles (Ag-NPs) synthesis

The aqueous extract of *C. rotundus* (0.1 g/mL) was prepared by immersing 1 g of finely ground churna in 10 mL of double-distilled water. The mixture was heated at 80 °C for 1 h in a temperature-controlled water bath. After cooling, the solution was filtered using Whatman filter paper to obtain a clear extract, which was stored in a clean container under refrigeration. For the synthesis of nanoparticles, silver nitrate ($AgNO_3$) served as the precursor salt. A 10 mL solution of 10 mM $AgNO_3$ was combined with 2 mL of the aqueous churna extract under constant stirring (500–600 rpm) at 60 °C for 1 h using a magnetic stirrer. The resulting solution was then centrifuged at 10,000 rpm using a cooling centrifuge. The silver nanoparticles (Ag-NPs) were subsequently dried and collected[25].

Analytical characterization of Ag-NPs

Characterization of the nanoparticles was carried out to assess their particle size distribution, shape, stability, crystallinity, zeta potential, and aggregation using various analytical techniques.

UV–visible spectrometric analysis

Preliminary characterization of the optical properties and the complete reduction of silver ions was carried out using a UV–visible spectrometer by recording their absorbance spectra. The surface plasmon resonance (SPR) shift was observed in the 200–800 nm wavelength range using a UV–visible spectrometer, with samples prepared by diluting double-distilled water tenfold.

Fourier-transformed spectrometric analysis

FT-IR analysis was performed with an ATR FT-IR Spectrometer (Jasco-4200, USA) over a 4000–400 cm^{-1} scanning range to identify functional groups and chemical interactions.

Scanning electron microscope analysis (SEM)

Surface morphology was characterized through scanning electron microscopy (SEM) using a Nova Nanosem 450, where samples were spread on adhesive carbon tape mounted on aluminum stubs, coated with a thin layer of gold, and examined at 20 kV.

XRD analysis

The crystallinity of the synthesized Ag-NPs was analyzed using X-ray diffraction (XRD) (Rigaku Ultima IV). The green-synthesized silver nanoparticles, in their dried powdered form, were examined over a 2θ range of 10°–70° at a scan rate of 10°/min, with operating conditions set to 40 KV and 30 mA.

Zeta potential and DLS

Zeta potential analysis was conducted to determine particle size and evaluate electrostatic interactions between nanoparticles and bioactive substances, providing insights into surface charge and stability.

Hydrogel formulation

Carbopol 974P (0.5%) powder was dispersed in double-distilled water and allowed to swell overnight to prepare the nano-gel. After thorough blending, 10 mg of the synthesized silver nanoparticles were incorporated into the Carbopol dispersion. Triethanolamine was added as a neutralizing agent to adjust the pH to 6.5 ± 0.5. The mixture was gently stirred during neutralization until a uniform and homogenous gel was formed[26].

Hydrogel characterization

The physical and chemical properties of the Ag-NPs loaded hydrogel were evaluated using several analytical techniques. The pH determination was conducted with a SYSTRONICS Digital pH Meter 335, where the glass and reference electrodes were fully submerged in the gel system to measure the pH accurately using a calibrated device. Viscosity was assessed using a Brookfield Viscometer DV-II+ Pro by pouring the gels into the sample holder and recording the viscosity at different rotational speeds. Gel strength was evaluated using a measuring cylinder and a 20 g device. A 50 g sample of hydrogel was placed in the cylinder at room temperature (25.5 °C), and the device was positioned on top. The gel strength was determined by recording the time (in seconds) it took for the device to sink 5 cm into the gel[27]. The Spreadability of the gels was measured by placing 0.2 g of gel in a 2 cm diameter circle on a glass plate, covering it with another plate, and applying a 200 g weight for five minutes. The spread area was then measured, and spreadability was calculated using the formula $\%S = A/x \times 100$, where S is spreadability, where A is the maximum spread area, and x is the gel weight[27]. Transparency was visually evaluated by placing 5 mL of the gel in a glass petri dish. Phase-separation studies were conducted by storing the prepared gels in containers under refrigeration overnight and then reversing the containers to check for separation, indicating interfacial tension fluctuations influenced by solvent or temperature. Finally, FT-IR analysis of the hydrogel and plain Carbopol gels was performed using the FT/IR-4600 type ATR PRO ONE spectrometer, scanning a range of 399.193 cm^{-1} to 4000.6 cm^{-1} to identify functional groups and chemical interactions.

In-vitro safety and efficacy study

Antibacterial activity (growth kinetic study)

For assessing the growth kinetics study of the hydrogel, the gram-positive strain *S. aureus*-MTCC 96 and the gram-negative strain *E. coli*-MTCC 443 were selected based on their clinical relevance in wound infections. Both strains are commonly used standard models in antimicrobial studies to evaluate the efficacy of antimicrobial agents[28]. For the study, a loopful of bacterial culture was collected from a slant and inoculated into the nutrient broth, followed by incubation overnight at 37 °C with shaking at 120 rpm. Stock solutions of Ag-NP hydrogel were prepared. For the growth kinetics study, reaction mixtures without the hydrogel were set up in a 96-well plate to assess bacterial growth both in the presence and absence of the hydrogel. Each reaction mixture contained 20 µL of bacterial culture, with the total volume adjusted to 300 µL using the nutrient broth. Different concentrations of the Ag-NPs loaded hydrogel (25, 50, 100, 250, and 500 µg/mL) were tested. Growth kinetics were monitored using a Biorad iMark Plate Reader by measuring optical density (OD) at 600 nm over 14 h[28].

Anti-inflammatory study

The in vitro anti-inflammatory activity was assessed using the protein denaturation method. For that, 0.02 mL of the sample solution, at varying concentrations (5–100 µg/mL) of synthesized Ag- NPs and Ag-NP embedded hydrogel, was separately mixed with 0.2 mL of bovine serum albumin (BSA) solution (1% w/v) and 4.8 mL of phosphate buffer solution (PBS, pH 6.4). The mixture was incubated at room temperature for 20 min, then heated at 57 °C for 20 min. After cooling, turbidity was measured at 660 nm using a UV-Vis spectrophotometer. The percentage inhibition of protein denaturation was calculated, with Diclofenac sodium serving as the standard reference drug[29].

Antioxidant activity

The antioxidant activity of the samples was evaluated in vitro using the DPPH (1,1-diphenyl-2-picrylhydrazyl) free radical scavenging method, with ascorbic acid serving as the reference standard. For the assay, 2 mL of DPPH methanolic solution (0.1 mM) was combined with 3 mL of the Ag-NPs or Ag- NP embedded hydrogel solution at different concentrations (10, 25, 50, 75, and 100 µg/mL). The mixture was incubated in the dark for 30 min to ensure completion of the reaction. The absorbance was then recorded at 517 nm using a UV-Vis spectrophotometer, and the IC50 value was calculated based on the ascorbic acid standard curve[30].

Cytotoxicity study

The viability of HEK293 was assessed using the MTT assay. Cells were cultured until they reached 70–80% confluency, then trypsinized, and 5000 cell per well were seeded into a 96-well plate. The cells were treated with Ag-NPs, and the hydrogel for 24, 48, and 72 h at 37 °C in a 5% CO_2 incubator. After the treatment, the media were removed, and the cells were washed with phosphate-buffered saline (PBS). Fresh medium (180 µL) and MTT solution (20 µL, 5 mg/mL in PBS) were added to each well, and the cells were incubated for 4 h at 37 °C in a 5% CO_2 environment. Following incubation, the medium and MTT solution were discarded, and the resulting purple formazan crystals were dissolved by adding 200 µL of absolute DMSO per well. The plates were kept at room temperature for 2 h to ensure complete dissolution. The absorbance of the dissolved formazan was measured at 570 nm using a Synergy H1 multi-mode microplate reader (BioTeK)[31,32].

Wound scratch assay

The scratch wound healing assay is a widely employed and versatile in vitro technique for assessing cell migration and proliferation under diverse experimental conditions, including gene knockdown and chemical treatments. In this method, a "wound" or gap is created in a confluent monolayer of cells using a sterile pipette tip, and the subsequent cell migration and growth into the gap are monitored over time to evaluate wound closure. This assay is simple, cost-effective, and easily customizable, with the potential for high-throughput adaptation using automated systems. In the present study, Human Dermal Fibroblasts (HDF) sourced from HiMedia, India, were cultured in high-glucose DMEM supplemented with 10% fetal bovine serum and 1% antibiotic-antimycotic solution. Cells were maintained at 37 °C in a CO_2 incubator with 5% CO_2 and 18–20% O_2. Passage 15 cells were

seeded at a density of 0.25 million per well in a 6-well plate and cultured to 80–100% confluence. A cross-shaped scratch was then carefully made using a sterile 200 µL pipette tip without changing the medium. Detached cells were removed by gentle washing, and the remaining cells were treated with the desired test compounds and incubated for an additional 48 h. Images of the wound area were captured at various time points (0, 24, 48, and 72 h) using consistent microscope settings. Wound closure was quantitatively analyzed using ImageJ software, with multiple fields per well documented to reduce variability, and all experiments were conducted in replicates to ensure reliability[33,34].

In-vivo efficacy study

All animal experiments were conducted in accordance with the Animal Research: Reporting of In Vivo Experiments (ARRIVE) guidelines. The Institutional Animal Ethics Committee of School of Pharmaceutical Sciences (Approval number: IAEC/SPS/SOA/04/2021) has approved the protocol, and this guidelines were strictly followed throughout the experiments.

Skin tolerance test

Skin tolerance test was performed using the OECD guideline 404 with slight modifications. Fur from the backs of all animals was removed from different sites using hair removal cream before 24 h. 0.5 g of formulated hydrogel was evenly and gently applied in a test site while untreated skin areas served as the control. The test sites were examined critically at 1 h after removing the test material and at 24 h, 48 h, 72 h, 7th, and 15th day for any dermal reaction[35].

Wound healing study (excision model)

Male Wistar rats weighing 200–250 g were obtained from the institutional animal house for this experiment. The rats were housed in a controlled environment with a 12-hour light/dark cycle and an ambient temperature of 23 °C ± 2 °C. Anaesthesia was administered intraperitoneally using a ketamine (90 mg/kg) and xylazine (10 mg/kg) mixture. The dorsal skin of the rats was depilated and disinfected with Hexa-sept solution. Full-thickness circular wounds, 5 mm in diameter, were surgically excised under aseptic conditions using a sterile dermal biopsy punch. Full-thickness incisions were made up to the loose subcutaneous tissue using surgical scissors. The rats were divided into five groups ($n = 6$), with treatments assigned as follows: Group 1 (standard treatment), Group 2 (no treatment), and Group 3 (Ag-NPs-loaded hydrogel). Daily photographs were taken using a digital camera to monitor wound contraction, ensuring the camera was positioned perpendicularly to the wound surface at a consistent distance. The rate of wound contraction was calculated as a percentage reduction from the initial wound size using the following formula:

% of wound contraction= (initial wound size) – (final wound size) ÷ (initial wound size) × 100.

Skin tissue samples of the wounds were taken on the 1st day and 17th day of the study. They were kept in a formalin solution (40%) for the histopathology study. Newly generated epithelial tissues and hair follicles were studied[36].

Statistical analysis

All experimental results are presented as the mean ± standard deviation (SD). Statistical comparisons between groups were conducted using the one-way ANOVA with the help of online software astatsa.com, with significance thresholds defined as ($^{**}p < 0.01$).

Results and discussion

Ag-NPs synthesis

Due to the Surface Plasmon Resonance (SPR) vibrations, after 30 to 60 min of adding the silver nitrate salt solution to the extract, a colour change from rust orange to dark brown was observed during the stirring process. The phytochemicals present in the C. rotundus extract were thought to reduce the silver to Ag-NPs. This shift of colours confirmed the reduction of Ag^{+} ions, leading to Ag-NP synthesis successfully. The synthesis of Ag-NPs from the *Cyperus rotundus* roots is represented in a pictorial form in Fig. 1.

Analytical characterization of Ag-NPs

The primary confirmation of Ag-NP synthesis was done with the help of a UV-visible spectrophotometer. Due to surface plasmon resonance, the maximum absorption peaks were observed at 422 nm, confirming nanoparticle synthesis[37].

Furthermore, its functionality was confirmed using an ATR FT-IR in the range of 400–4000 cm^{-1} as given in Fig. 2 The spectrum embellishes the peaks 3747.98 cm^{-1}, which denotes the stretching of O–H, while the peaks that are present at 1650 cm^{-1} and 1537 cm^{-1} illustrate the C=O and N–O stretching correspondingly. The N–O bond describes the stretching of the Nitro group in the solution. The clear peak of C–H bending depicts aldehyde groups, and the peaks at 870.70 cm^{-1}, 825 cm^{-1}, and 776 cm^{-1} indicate the presence of Alkene due to the bending of C=C. These groups have a strong affinity with Ag, which plays an important role in reducing and capping silver ions. The 531 cm^{-1} peak in the IR spectrum denotes the presence of an Ag-O bond, which confirms the formation of Ag-NPs[38].

The SEM analysis enables the detailed examination of the morphological structure of the synthesized Ag-NPs. The finding presented in Fig. 3A indicates the non-uniform distribution of the synthesized particles in a spherical shape, which resembles the aggregation of synthesized nanoparticles.

X-ray diffraction (XRD) analysis is a valuable technique for assessing the crystallinity of synthesized silver nanoparticles (Ag-NPs). The intensity and positions of the diffraction peaks confirm their crystalline nature. As demonstrated in Fig. 4., Peaks observed at 32.28°, 46.3°, 64.74°, and 77.32° correspond to the characteristic

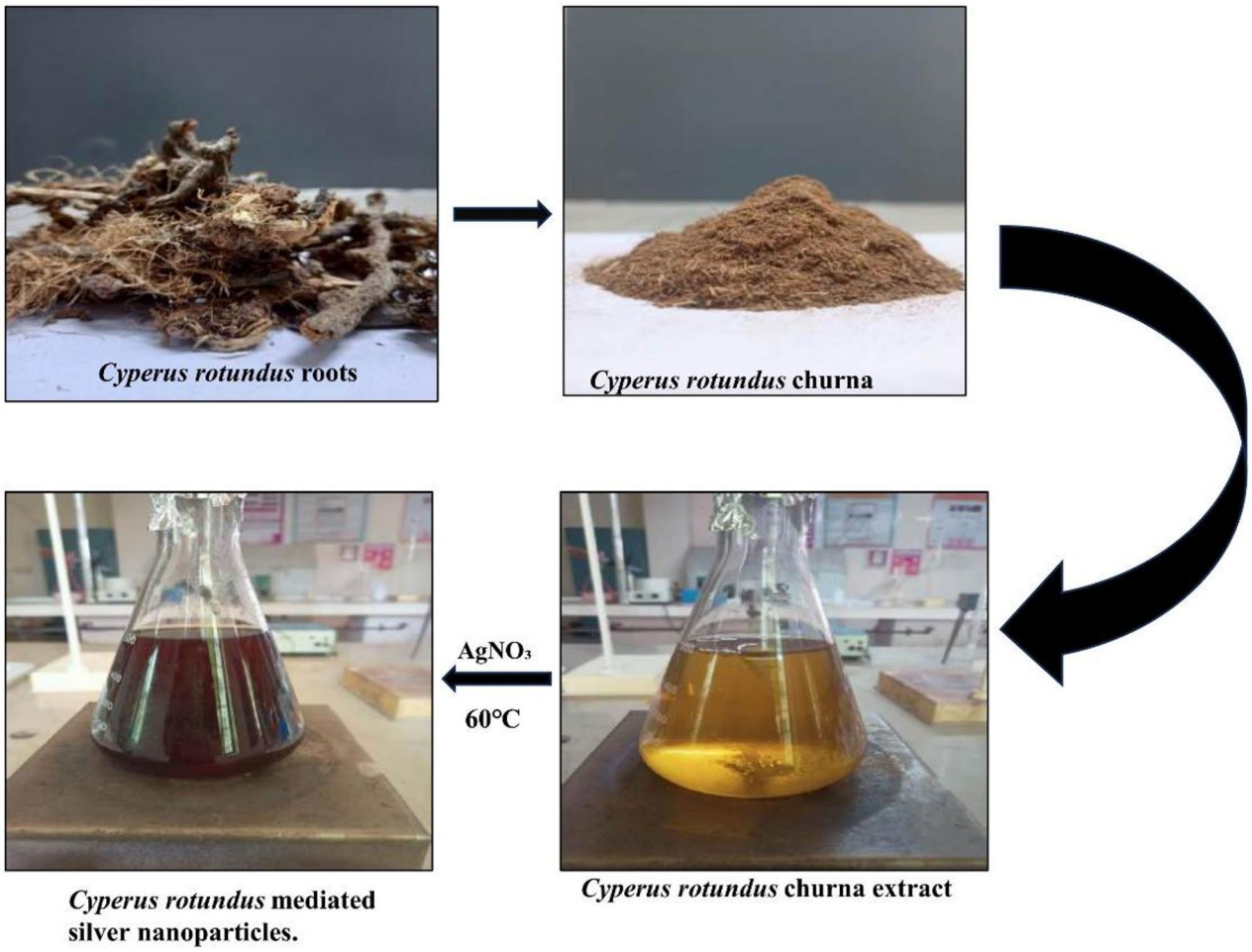

Fig. 1. The method of green synthesis of *C. rotundus-mediated* silver nanoparticles.

face-centered cubic (FCC) structure of the green-synthesized Ag-NPs. Using the Debye-Scherrer equation, the average crystallite size of the Ag-NPs was calculated to be approximately 288.52 nm[39,40]. The crystallite size of 288.52 nm is notably larger than the typical range expected for silver nanoparticles. This anomaly is most likely due to nanoparticle aggregation, a common occurrence in green synthesis methods where plant-derived biomolecules serve as reducing and capping agents. While these biomolecules offer eco-friendly synthesis, they may not always provide adequate steric or electrostatic stabilization, leading to particle agglomeration. Additionally, aggregation may occur during the storage period prior to XRD analysis[41]. It's also important to note that crystallite size derived from XRD using the Debye–Scherrer equation represents the dimensions of coherent diffraction domains, which may not directly correspond to the actual particle size observed through microscopic techniques. Overlapping of nanoparticles or forming nanoclusters could also contribute to this discrepancy. Thus, the large crystallite size likely reflects aggregated nanoparticle clusters rather than discrete individual particles[42–44]. Zeta potential analysis was performed to evaluate the surface charge and dispersity of the nanoparticles. The DLS-Zeta analysis revealed that the average particle size was 633 nm, which was attributed to the slight agglomeration of the Ag-NPs. As per DLS, the storage of the sample before analysis or the phytoconstituents from *C. rotundus* acting as natural capping agents may have an impact on agglomeration in solution, which is most likely the cause of the DLS data indicating a greater size (633 nm). The hydrodynamic radius may be increased by these surface-bound biomolecules, which could cause DLS measurements to overestimate the true size of the nanoparticle[42,45]. However, as per the results of Zeta potential, it confirmed that the Ag-NPs exhibited a surface potential of − 13.98 mV with a polydispersity index of 0.483, indicating good dispersion of the particles.

Formulation and characterization of the Ag-NPs loaded carbopol hydrogel

The Ag-NPs were loaded on a 0.5% Carbopol hydrogel for topical application, as shown in Fig. 5. Carbopol 974, a polyacrylic acid derivative, contains polymer chains rich in carboxyl (-COOH) and hydroxyl (-OH) functional groups. When hydrated to form a hydrogel, these functional groups can chelate with silver ions (Ag^+), promoting the stabilization and uniform dispersion of silver nanoparticles (Ag-NPs) within the gel matrix[46].

This hydrogel system was characterized in terms of its physicochemical and mechanical properties. As this hydrogel was planned to be applied to the skin, its pH should be near the skin's pH. The pH of the hydrogel was

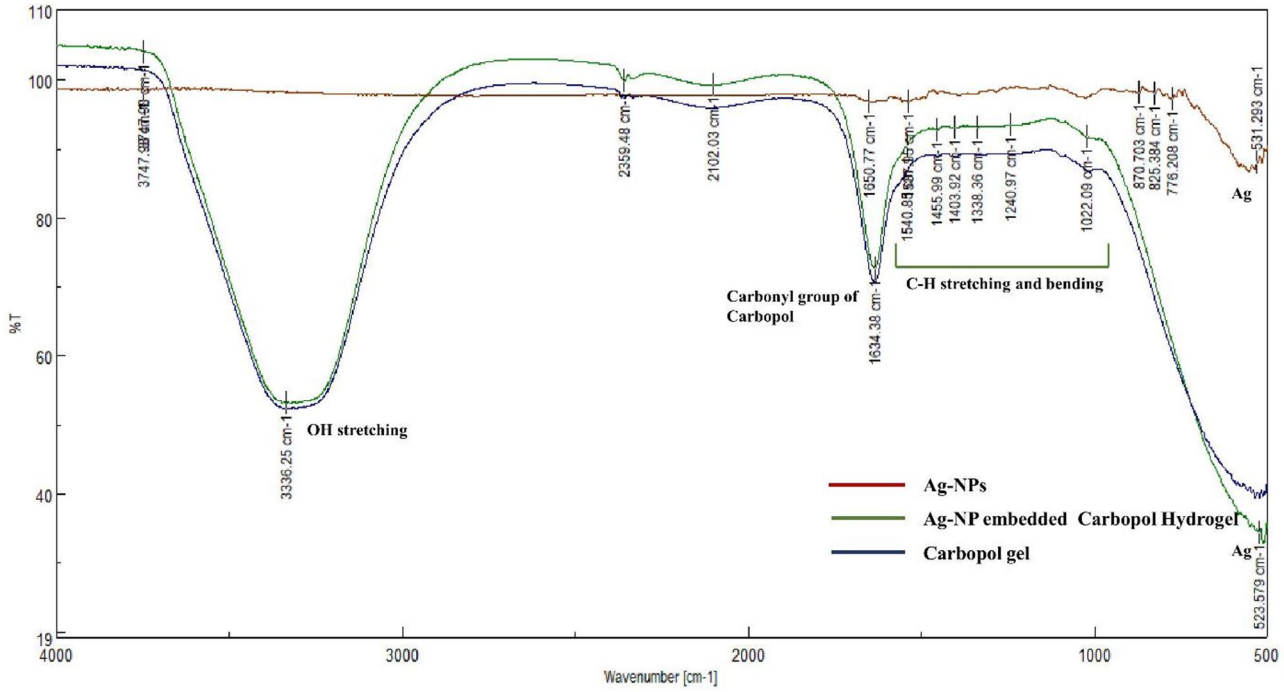

Fig. 2. FT-IR spectrum of synthesized Ag-NP embedded hydrogel, Carbopol gel, and Ag-NPs.

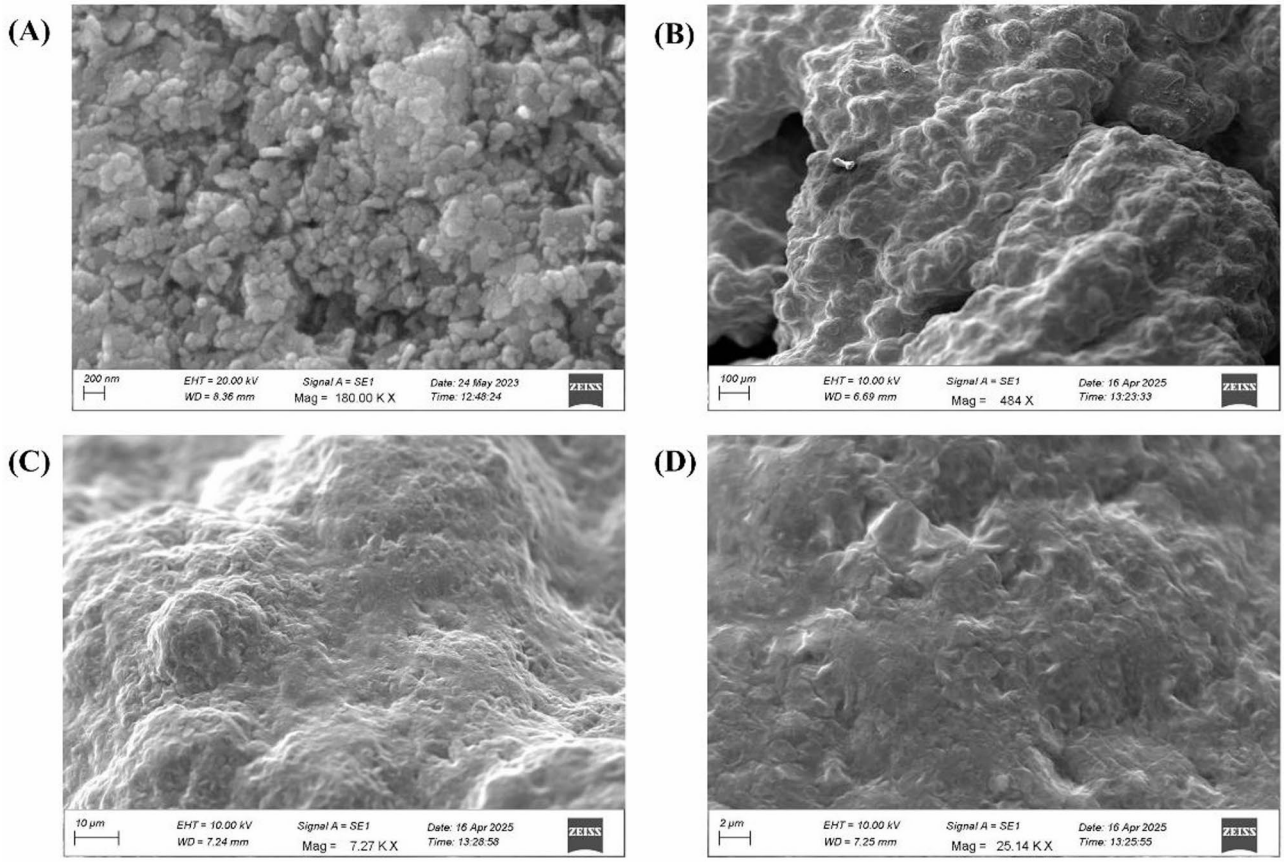

Fig. 3. SEM Analysis of *C. rotundus*-mediated silver nanoparticles and Ag-NP embedded hydrogel, where (**A**) SEM image for Ag-NPs, and (**B**–**D**) for hydrogel in different scales.

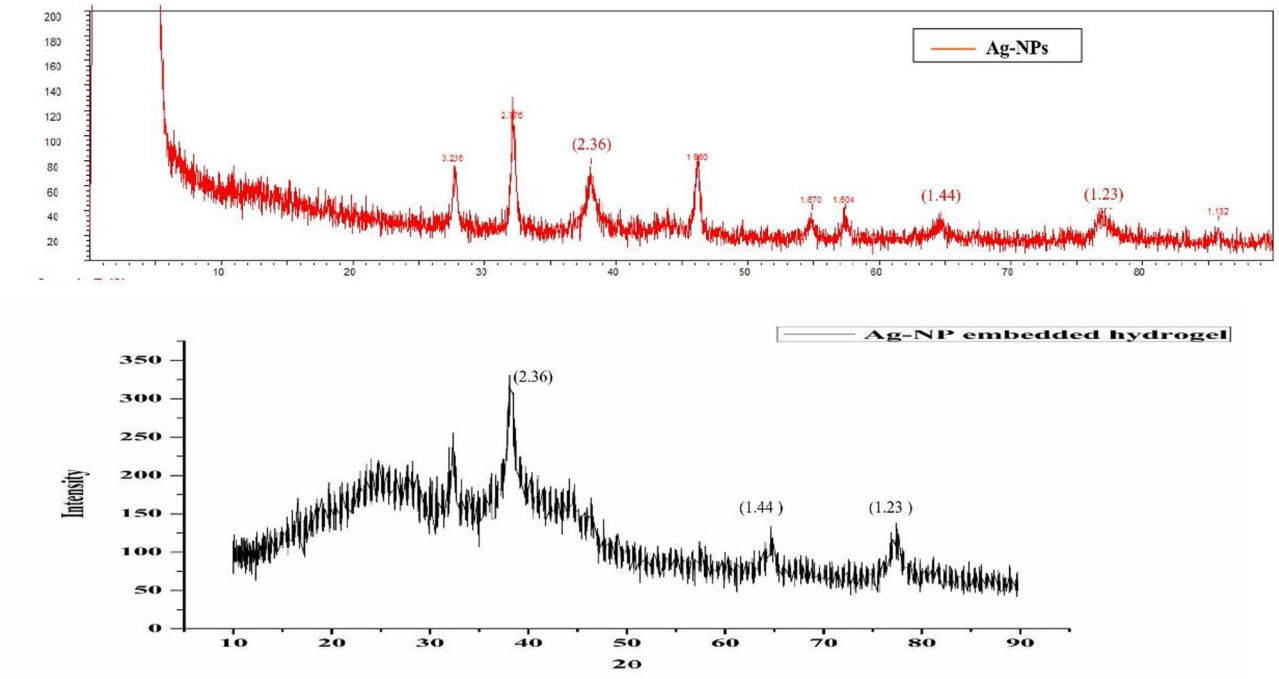

Fig. 4. XRD Analysis of *C. rotundus*-mediated silver nanoparticles and Ag-NP embedded hydrogel.

Fig. 5. Visual representation of Ag-NP embedded hydrogel.

measured using a calibrated pH meter and found to be 5.8. Since this is close to the skin's natural pH, the gel can be used topically without irritating. The transparency of the formulated hydrogel was determined using a UV–visible spectrophotometer, where the % transmittance was 14.13% at 600 nm and 25.25% at 800 nm. This lesser transmittance indicated lesser transparency of the product. A less transparent gel can serve as a more

effective physical barrier against external contaminants, thereby providing enhanced protection to the wound bed and reducing the risk of infection[47]. The viscosity was measured using a Brookfield Viscometer, which was found to be 70,070 ± 1 cP, indicating high viscosity. This high viscosity led to the formulation's good retention on the skin, which will create a protective barrier for external factors, minimizing infection, and providing a moist environment to the wound bed. The formulation's gelling strength was determined by observing the time taken to sink the hydrogel up to 5 cm, and it took 164 ± 1.2 s, which means the hydrogel has good retentionability on the wound site, minimizing runoff and enhancing localized treatment. The hydrogel possessed suitable spreadability properties as the spreadability factor came to 268 ± 0.02 g.cm.min^{-1}, indicating favorable application characteristics for wound. This supports even application over the irregular surface of the wound, providing patient comfort and dosing consistency. Additionally, the phase separation study was performed to identify the interfacial tension fluctuation, which may be affected by the solvent and temperature. After overnight observation, no change was found in the formulation, which confirmed the compatibility between the Ag-NPs and Carbopol hydrogel. An FT-IR analysis of Ag-NPs loaded hydrogel, Ag-NPs, Carbopol hydrogel, and Ag-NP embedded hydrogel (Fig. 2) was performed to examine potential interactions. The broadening of the peak at 3336 cm^{-1} indicates the OH stretching in the hydrogel, indicating water entrapment in the hydrogel network. C–H stretching and bending appeared in the range of 1540–1000 cm^{-1}. Moreover, the peak at 1634.38 cm^{-1} indicates the carbonyl group of Carbopol in both spectra of Carbopol gel and Ag-NP embedded hydrogel[48]. No new peaks indicating chemical interactions were observed, suggesting physical embedding of the nanoparticles. However, the presence of the characteristic Ag peak in the spectra, slightly shifted due to interactions with the hydrogel matrix, confirms the successful incorporation of AgNPs into the Carbopol hydrogel, as shown in Fig. 2.

Additionally, SEM and XRD analyses of the hydrogel were performed, as shown in Fig. 3B–D and Fig. 4, respectively. SEM images demonstrated the homogeneous distribution of Ag-NPs throughout the porous network of the hydrogel. The XRD pattern exhibited both sharp and broad peaks, indicating the coexistence of crystalline Ag-NPs embedded within the amorphous Carbopol structure.

In-vitro activity study

Growth-kinetics profile of Ag-NPs loaded hydrogel

Silver nanoparticles (AgNPs) are well-documented for their potent antibacterial activity, primarily through direct interaction with bacterial cell membranes. This interaction compromises membrane integrity, increasing permeability and resulting in the leakage of intracellular contents. Beyond physical disruption, AgNPs also generate reactive oxygen species (ROS), which induce oxidative stress and damage vital biomolecules, including lipids, proteins, and DNA. Additionally, silver ions (Ag^{+}) released from the nanoparticles bind to thiol groups in bacterial enzymes, disrupting key metabolic processes and ultimately leading to cell death. These mechanisms are especially effective against Gram-negative bacteria due to their unique outer membrane structure, which renders them more susceptible to nanoparticle penetration[49].

To evaluate the antimicrobial efficacy of the hydrogel system, a growth kinetics study was performed using *Escherichia coli* and *Staphylococcus aureus*. Optical density (OD) was measured hourly over a 14-h period using a plate reader, and the data are presented in Fig. 6. The results show that bacterial proliferation occurred during the initial 6 h; however, a gradual decline in growth was observed thereafter. This trend confirms the inhibitory effect of the hydrogel on both *E. coli* and *S. aureus*, demonstrating its antimicrobial potential.

Anti-inflammatory activity

Inflammation plays a critical role in the wound-healing process, but excessive inflammation can prolong the healing phase or lead to chronic wounds[50]. Therefore, the anti-inflammatory potential of Ag-NPs was assessed to evaluate their ability to reduce inflammation during wound healing. The anti-inflammatory activity of both the Ag-NPs and the hydrogel was measured using a protein denaturation assay with bovine serum albumin (BSA), employing diclofenac sodium as the standard drug for comparison. The results demonstrated (Fig. 7A) that both Ag-NPs and hydrogel effectively inhibited protein denaturation, achieving 73.43% and 74.82% inhibition at the highest tested concentration (100 µg/mL), with an IC_{50} value of 62.2 µg/mL for Ag-NPs and hydrogel at 59.17 µg/mL. Ag-NPs exert anti-inflammatory effects by downregulating the production of key

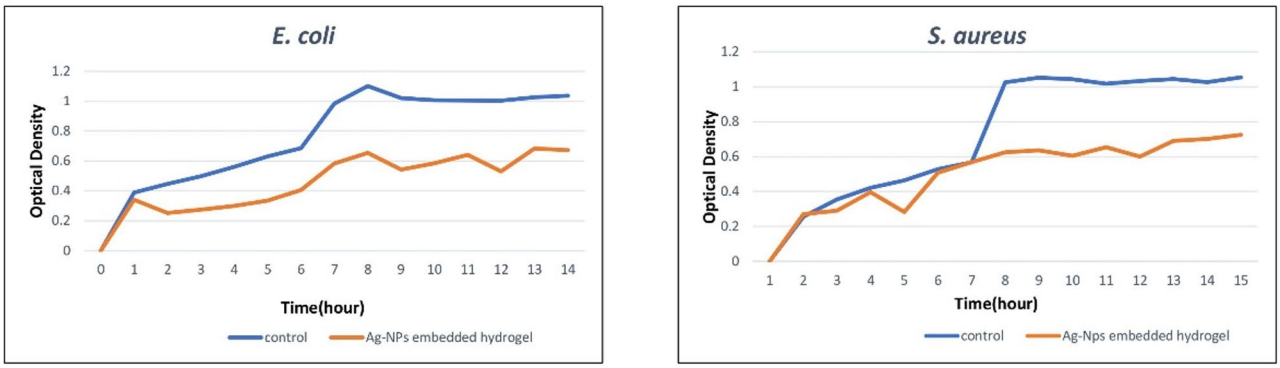

Fig. 6. Growth kinetics profile of *E. coli*, *S. aureus*.

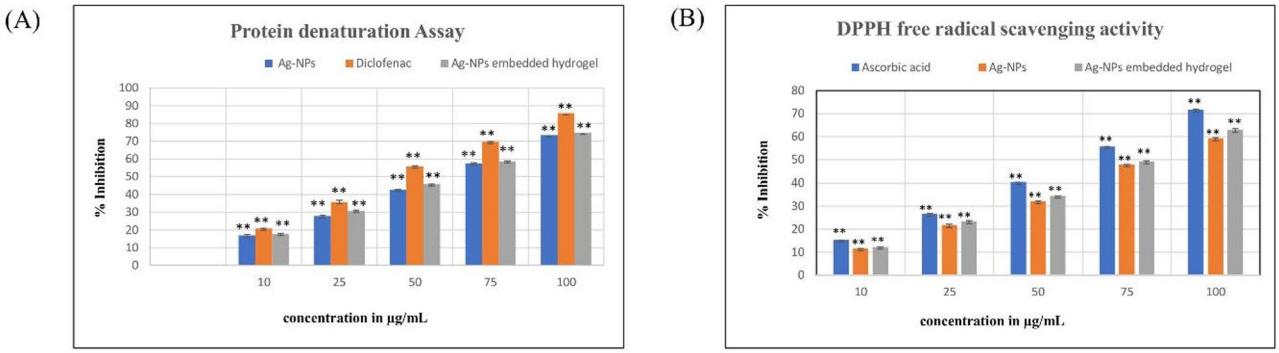

Fig. 7. In vitro biological activity studies of Ag-NPs and Ag-NP embedded hydrogel. (**A**) protein denaturation assay, (**B**) Free radical scavenging assay, where $^{**}p < 0.01$.

pro-inflammatory cytokines, including TNF-α, IL-6, and IL-1β. They also inhibit the activation of the NF-κB signaling pathway, a central regulator of the inflammatory response. By modulating these pathways, Ag-NPs help reduce excessive inflammation at the wound site, promote tissue regeneration, and create a more favorable environment for healing[51]. These findings suggest that Ag-NPs, along with the formulation, possess significant anti-inflammatory properties, potentially aiding in inflammation regulation during the wound healing process.

Free radical scavenging activity

Compounds often exhibit antioxidant properties that protect cells from free radicals, which are generated by the formation of unpaired electrons in oxygen (O_2^-). These free radicals can interact with biomolecules, leading to significant cellular damage. During wound healing, free radicals contribute to oxidative stress, tissue damage, and prolonged inflammation, which delays the healing process[52]. In this study, the free radical scavenging activity of Ag-NPs and Ag-NP-embedded hydrogel was assessed using the DPPH radical scavenging assay, with ascorbic acid used as the standard drug. The IC50 values of ascorbic acid, Ag-NPs, and Ag-NP embedded hydrogel were 65.31 µg/mL, 81.2 µg/mL, and 76.56 µg/mL, respectively (Fig. 7B). The results demonstrate that the Ag-NPs possess significant reducing potential in neutralizing free radical species. At the same time, the formulation also exhibits potent free radical scavenging activity, indicative of better antioxidant properties.

Cell viability assay

Silver nanoparticles exhibit a unique combination of physical and chemical properties, making them highly reactive and effective at inhibiting various microorganisms. However, this same reactivity can also result in cytotoxic effects on noncancerous cells[53]. In this study, we aimed to synthesize a safer variant of silver nanoparticles using *C. rotundus*. The biocompatibility of the synthesized Ag-NPs was assessed by evaluating their effects on the viability of human embryonic kidney (HEK293) cells over a 72-h exposure period. The results demonstrated in Fig. 8A show 98% cell viability of Ag-NPs, and Fig. 8B shows 92% of Ag-NP embedded hydrogel at a concentration of 1000 µg/mL after 72 h, indicating that these Ag-NPs, along with the hydrogel, are safe for use up to this concentration.

Wound scratch assay

Overall, the wound healing study demonstrated that the Ag-NP embedded hydrogel effectively promoted wound closure in HDF cells and exhibited significant angiogenic activity as shown in Fig. 9A. In the control group, 70.52% of wound closure was observed after 72 h of incubation. In contrast, both Cipladine (1 mg/mL) and the Ag-NP embedded hydrogel (1 mg/mL) achieved complete (100%) wound closure within the same period. The Ag-NP hydrogel significantly accelerated wound healing in a time-dependent manner, comparable to the standard reference drug, Cipladine. The covered wound area and % wound closure has been given in Fig. 9B,C, respectively.

In conclusion, treatment with Hydrogel effectively enhanced wound healing in HDF cells in a time-dependent manner, with notable improvements observed at 48 and 72 h. This treatment significantly promoted fibroblast migration and confirmed its angiogenic potential, highlighting its relevance for skin tissue regeneration.

Skin tolerance test

Skin tolerance tests were conducted, and the test sites were examined for any dermal reactions 1 h after removing the test material and at 24 h, 48 h, 72 h, the 7th day, and the 15th day. No dermal reactions or redness were observed in the animals during these evaluations.

Wound healing study

The wound healing study was performed in the excision wound model by taking three groups of rats. All the rats were examined for 17 days. In Fig. 8C, Group 1 represents the control group, where no treatment was given to the wounded rats. Group 2 is the positive control group, treated with the standard drug (mupirocin). The third group is the treatment group, which received the Ag-NP-loaded hydrogel. From the table above, it is visible that the prepared hydrogel exhibits a similar effect to the standard marketed treatment. The statistically

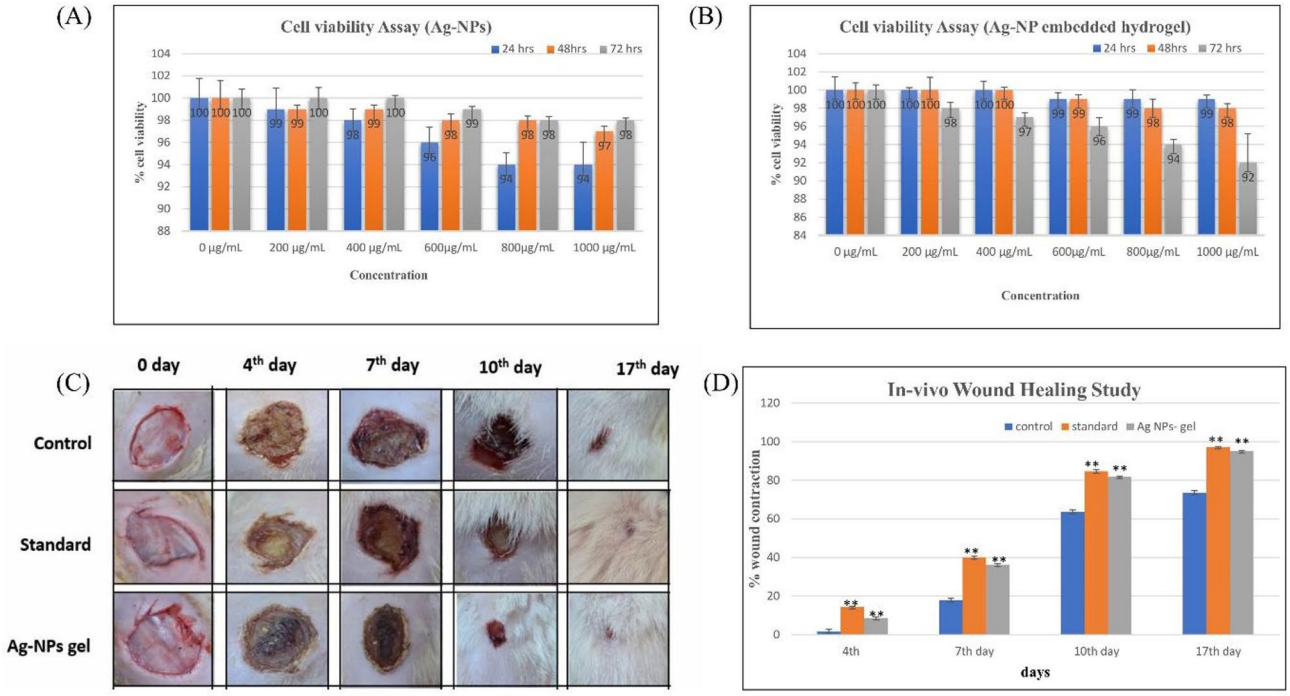

Fig. 8. Statistical representation for (**A**) cell viability of Ag-NPs, (**B**) cell viability of Ag-NP embedded hydrogel, (**C**) Pictorial representation of wound healing study, and (**D**) statistical comparison of wound healing activity of Ag-NPs loaded Carbopol hydrogel.

significant difference of the test group was determined in comparison to a control group using one-way ANOVA. A comparative statistical significance graph of the % wound contraction (**$p < 0.01$) is demonstrated in Fig. 8D.

Histopathology

In Fig. 10, group A represents the standard group that received Mupirocin ointment therapy, Group B serves as the untreated control group, Group C represents the treatment with Ag-NPs loaded hydrogel on the seventeenth day, and Group D represents normal skin. The figures clearly illustrate the pattern of new skin formation in each group. The area covered with black dotted lines represents the re-epithelialization of the wounded skin of different groups. Black arrows indicate epithelial cells, while orange arrows signify hair follicles. In Group A, epithelial tissue and hair follicles are distinctly visible, indicating significant new skin regeneration. Similarly, Group C, the test group, demonstrates notable regeneration, with well-formed epithelial tissue and hair follicles. These findings suggest that our formulation potentiated the wound site, providing favorable results in skin formation. In contrast, Group B exhibits fewer epithelial tissues and hair follicles than the other groups, highlighting its slower healing process. To ensure objective assessment, histopathological images from all treatment groups were analyzed for re-epithelialization using ImageJ software. Epithelial thickness at the wound site was measured, and the percentage of re-epithelialization was calculated using the formula: Re-epithelization [distance of axis covered by epithelium (a) + (b)]/[distance of minor axis between original wound edge (c)] ×100. Based on this analysis, re-epithelialization percentages were found to be 92% for Group 1 (mupirocin-treated), 68% for Group 2 (untreated), and 86% for Group 3 (Ag-NP embedded hydrogel-treated). All groups demonstrated partial re-epithelialization (score = 1, as values were below 95%). However, both the standard treatment and test groups exhibited substantially greater re-epithelialization compared to the untreated group, indicating effective wound coverage and healing response[54].

Conclusion

This study successfully synthesized silver nanoparticles using an eco-friendly green synthesis approach with *C. rotundus* and formulated a biocompatible Carbopol-based hydrogel for wound healing. The AgNP-loaded hydrogel exhibited significant antibacterial efficacy, reduced inflammation, and accelerated wound healing, demonstrating comparable performance to standard treatments. Importantly, cytotoxicity evaluations confirmed the formulation's safety, addressing concerns related to silver ion toxicity. Given the increasing prevalence of MDR bacteria and the growing demand for safe and effective wound management strategies, this AgNP-loaded hydrogel presents a viable and safer alternative to conventional treatments.

In contrast to commercial wound healing formulations, which frequently depend on synthetic antibiotics or chemical antiseptics, this AgNP-loaded hydrogel presents a potentially safer alternative, particularly in the context of increasing antibiotic resistance. Although some commercial products incorporate silver, worries about silver ion toxicity and the potential for argyria persist. Our green synthesis method, employing *Cyperus rotundus* extract as a natural capping agent, seems to improve biocompatibility, a finding supported by in vitro

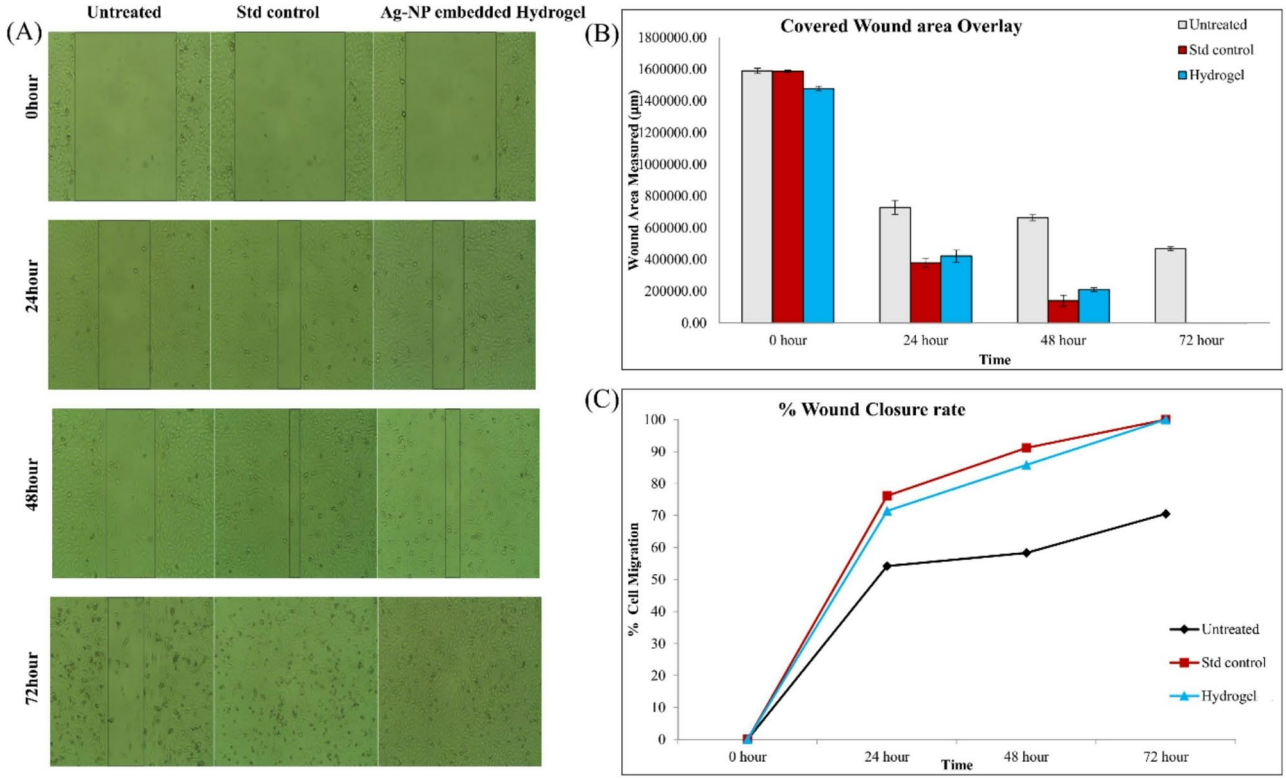

Fig. 9. (**A**) In-vitro wound healing activity of Ag-NP embedded hydrogel with 1 mg/ml at different time intervals of 0, 24, 48, and 72 h on Human dermal fibroblasts. In-vivo activity study (**B**) Overlaid bar graph represented the wound healing effect of Hydrogel against the HDF cells at different intervals in terms of wound area, and (**C**) Comparative scatter graph represented the wound healing effect of Hydrogel against the HDF cells at different intervals in terms of % wound closed area. Presented values were the average of 5 independent individual experiments ($N = 5$).

safety assessments. This enhanced biocompatibility is likely attributable to the natural compounds within the extract, which reduce silver ion release and oxidative stress. Moreover, the AgNPs in our hydrogel demonstrate broad-spectrum antimicrobial activity, potentially lessening the reliance on conventional antibiotics and their inherent risks.

Although this study presents promising findings, its limitations include reliance on in vitro and animal models, which may not fully predict human outcomes. Additionally, the long-term stability, scalability of the green synthesis method, and potential for immune response or allergic reactions upon repeated applications were not explored. Further research, including comprehensive clinical trials and long-term safety evaluations, is essential to fully assess the therapeutic potential and facilitate the translation of this formulation for clinical use and commercialization. Nevertheless, this AgNP-based hydrogel, developed using *C. rotundus*, shows promise as a natural and potentially safer alternative for advanced wound care.

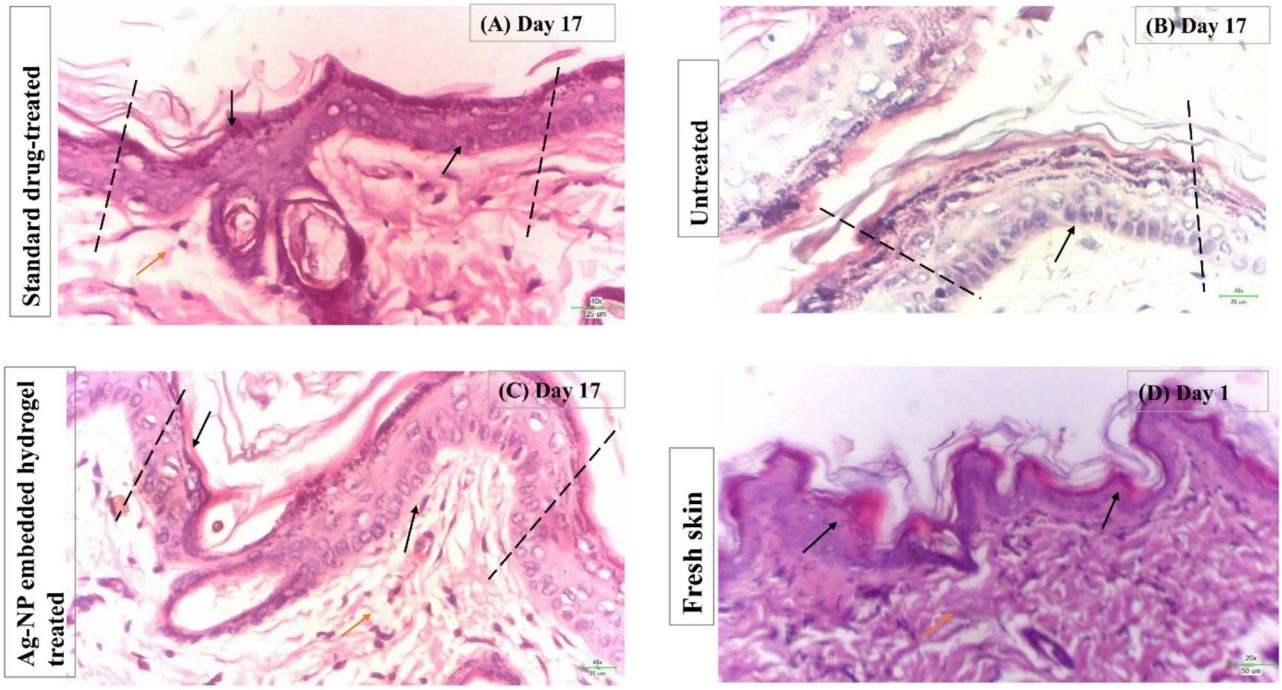

FIg. 10. Histopathology of the treatment groups.

Data availability

The datasets produced and/or examined in this study can be obtained from the corresponding author upon reasonable request.

Received: 14 March 2025; Accepted: 21 May 2025
Published online: 26 May 2025

References

1. Vijapur, L. S. et al. Wound healing potential of green synthesized silver nanoparticles of Glycyrrhiza glabra Linn root extract: A preclinical study. *JTEMIN*. 100214 https://doi.org/10.1016/j.jtemin.2025.100214 (2025).
2. Younis, N. S., Mohamed, M. E. & El Semary, N. A. Green synthesis of silver nanoparticles by the cyanobacteria synechocystis Sp.: characterization, antimicrobial and diabetic wound-healing actions. *Mar. Drugs*. **20**, 56. https://doi.org/10.3390/md20010056 (2022).
3. Sharma, D., Misba, L. & Khan, A. U. Antibiotics versus biofilm: an emerging battleground in microbial communities. *Antimicrob. Resist. Infect. Control*. **8**, 1–10. https://doi.org/10.1186/s13756-019-0533-3 (2019). DOI: HYPERLINK .
4. Hoang, T. P. N., Ghori, M. U., Ousey, K. & Conway, B. Current and advanced therapies for chronic wound infection: an overview of chronic wounds, including their physiology, causes and management options. *Pharm. J.* **309** https://doi.org/10.1211/PJ.2022.1.148212 (2022).
5. Parlet, C. P., Brown, M. M. & Horswill, A. R. Commensal Staphylococci influence *Staphylococcus aureus* skin colonization and disease. *Trends Microbiol.* **27**, 497–507. https://doi.org/10.1016/j.tim.2019.01.008 (2019).
6. Asvar, Z. et al. Enhancing antibacterial activity against multi-drug resistant wound bacteria: incorporating multiple nanoparticles into chitosan-based nanofibrous dressings for effective wound regeneration. *J. Drug Del. Sci. Tech.* **95**, 105542. https://doi.org/10.1016/j.jddst.2024.105542 (2024).
7. Baveloni, F. G. et al. Antimicrobial effect of silver nanoparticles as a potential healing treatment for wounds contaminated with *Staphylococcus aureus* in Wistar rats. *J. Drug Del. Sci. Tech.* **103**, 106445. https://doi.org/10.1016/j.jddst.2024.106445 (2025).
8. Bruna, T., Maldonado-Bravo, F., Jara, P. & Caro, N. Silver nanoparticles and their antibacterial applications. *Int. J. Mol. Sci.* **22**, 7202. https://doi.org/10.3390/ijms22137202 (2021).
9. Sofi, M. A., Sunitha, S., Sofi, M. A., Pasha, S. K. & Choi, D. An overview of antimicrobial and anticancer potential of silver nanoparticles. *J. King Saud Univ. Sci.* **34**, 101791. https://doi.org/10.1016/j.jksus.2021.101791 (2022).
10. Jaswal, T. & Gupta, J. A review on the toxicity of silver nanoparticles on human health. *Mater. Today Proc.* **81**, 859–863. https://doi.org/10.1016/j.matpr.2021.04.266 (2023).
11. Stozhko, N. et al. Green silver nanoparticles: Plant-extract-mediated synthesis, optical and electrochemical properties. *Physchem*. **4**, 402–419. https://doi.org/10.3390/physchem4040028 (2024).
12. Pradeep, M., Kruszka, D., Kachlicki, P., Mondal, D. & Franklin, G. Uncovering the phytochemical basis and the mechanism of plant extract-mediated eco-friendly synthesis of silver nanoparticles using ultra-performance liquid chromatography coupled with a photodiode array and high-resolution mass spectrometry. *ACS Sustain. Chem. Eng.* **10**, 562–571. https://doi.org/10.1021/acssuschemeng.1c06960 (2021).
13. Srivastava, R. K., Singh, A. & Shukla, S. V. Chemical investigation and pharmaceutical action of Cyperus rotundus-a review. *JBAPN*. **3**, 166–172. https://doi.org/10.1080/22311866.2013.833381 (2013).

14. Tongkasee, P. et al. Extraction and phytochemical profile of three herbal weeds: Chromolaena odorata L., Amaranthys Virdis L., and Cyperus rotudus L. for green synthesis of silver nanoparticles. *ASEAN J. Sci. Tech. Rep.* **26**, 10–23. https://doi.org/10.55164/ajstr.v26i3.249309 (2023).
15. Zhang, L. L., Zhang, L. F., Hu, Q. P., Hao, D. L. & Xu, J. G. Chemical composition, antibacterial activity of *Cyperus rotundus* rhizomes essential oil against *Staphylococcus aureus* via membrane disruption and apoptosis pathway. *Food Control.* **80**, 290–296. https://doi.org/10.1016/j.foodcont.2017.05.016 (2017).
16. Peerzada, A. M. et al. Traditional uses, phytochemistry, and pharmacological activities. *J. Ethnopharmacol.* **174**, 540–560. https://doi.org/10.1016/j.jep.2015.08.012 (2015).
17. Suman, T. Y., Rajasree, S. R., Kanchana, A. & Elizabeth, S. B. Biosynthesis, characterization and cytotoxic effect of plant mediated silver nanoparticles using *Morinda citrifolia* root extract. *Colloids Surf. B Biointerfaces.* **106**, 74–78. https://doi.org/10.1016/j.colsurfb.2013.01.037 (2013).
18. Sharma, S. K. & Singh, A. P. Antimicrobial investigations on rhizomes of *Cyperus rotundus* Linn. *Der Pharmacia Lettre.* **3**, 427–431 (2011).
19. Rao, P. D. Wound healing activity of cyperus rotundus Linn. *Indian J. Pharm. Sci.* **33**, 845 (1995).
20. Gounden, V. & Singh, M. Hydrogels and wound healing: current and future prospects. *Gels* **10**, 43. https://doi.org/10.3390/gels10010043 (2024).
21. Lin, X. et al. Hydrogels and hydrogel-based drug delivery systems for promoting refractory wound healing: applications and prospects. *Int. J. Biol. Macromol.* 138098 https://doi.org/10.1016/j.ijbiomac.2024.138098 (2024).
22. Hao, Y., Zhao, W., Zhang, H., Zheng, W. & Zhou, Q. Carboxymethyl chitosan-based hydrogels containing fibroblast growth factors for triggering diabetic wound healing. *Carbohydr. Polym.* **287**, 119336. https://doi.org/10.1016/j.carbpol.2022.119336 (2022).
23. Deng, L. et al. Bacterial cellulose reinforced chitosan-based hydrogel with highly efficient self-healing and enhanced antibacterial activity for wound healing. *Int. J. Biol. Macromol.* **217**, 77–87. https://doi.org/10.1016/j.ijbiomac.2022.07.017 (2022).
24. Wu, X. et al. Carbopol 940-based hydrogels loading synergistic combination of Quercetin and Luteolin from the herb Euphorbia humifusa to promote Staphylococcus aureus infected wound healing. *RSC Med. Chem.* **15**, 553–560. https://doi.org/10.1039/D3MD00611E (2024).
25. Jadhav, K., Dhamecha, D., Bhattacharya, D. & Patil, M. Green and ecofriendly synthesis of silver nanoparticles: characterization, biocompatibility studies and gel formulation for treatment of infections in burns. *J. Photochem. Photobiol. B.* **155**, 109–115. https://doi.org/10.1016/j.jphotobiol.2016.01.002 (2016).
26. Sood, R. & Chopra, D. S. Optimization of reaction conditions to fabricate Ocimum sanctum synthesized silver nanoparticles and its application to nano-gel systems for burn wounds. *MSE* **92**, 575–589. https://doi.org/10.1016/j.msec.2018.06.070 (2018).
27. Parhi, R., Goutam, S. V. S. & Mondal, S. Formulation and evaluation of transdermal gel of ibuprofen: use of penetration enhancer and microneedle: formulation and evaluation of transdermal gel of ibuprofen. *IJPS* **16**, 11–32. https://doi.org/10.22037/ijps.v16.40382 (2020).
28. Chatterjee, T., Chatterjee, B. K., Majumdar, D. & Chakrabarti, P. Antibacterial effect of silver nanoparticles and the modeling of bacterial growth kinetics using a modified Gompertz model. *BBA-GS* **1850**, 299–306. https://doi.org/10.1016/j.bbagen.2014.10.022 (2015).
29. Parmanik, A. et al. Development of Triphala Churna extract mediated iron oxide nanoparticles as novel treatment strategy for triple negative breast cancer. *J. Drug Del. Sci. Tech.* **76**, 103735. https://doi.org/10.1016/j.jddst.2022.103735 (2022).
30. Abdullah, J. A. A. et al. Green synthesis and characterization of iron oxide nanoparticles by Pheonix dactylifera leaf extract and evaluation of their antioxidant activity. *Sustain. Chem. Pharm.* **17**, 100280. https://doi.org/10.1016/j.scp.2020.100280 (2020).
31. Supino, R. MTT assays. In *In vitro toxicity testing protocols*, 137–149 (1995).
32. Jain, S. & Roy, I. Aptamer reduces aggregation of mutant Huntingtin and rescues proteostasis network in Non-Neuronal and neuronal cells. *ACS Chem. Neurosci.* **14**, 2385–2395. https://doi.org/10.1021/acschemneuro.3c00226 (2023).
33. Cory, G. Scratch-wound assay. *Cell. Migr. Dev. Methods Protoc.* 25–30. https://doi.org/10.1007/978-1-61779-207-6_2 (2011).
34. Liu, C. Y., Polk, D. B. & Frey, M. R. Mucosal restitution and repair. *GI Physiology*, 683–708 (Academic Press, 2018). https://doi.org/10.1016/B978-0-12-809954-4.00029-3.
35. Christou, N. V., Ing, A. F. M., Larson, D. L. & Meakins, J. L. A reliable rat model of the delayed hypersensitivity skin test response. *J. Surg. Res.* **37**, 264–268. https://doi.org/10.1016/0022-4804(84)90187-2 (1984).
36. Abdel-Gawad, R., Osman, R., Awad, G. A. & Mortada, N. Wound healing potential of silver nanoparticles embedded in optimized bio-inspired hybridized Chitosan soft and dry hydrogel. *Carbohydr. Polym.* **324**, 121526. https://doi.org/10.1016/j.carbpol.2023.121526 (2024).
37. Ali, I. A. M., Ahmed, A. B. & Al-Ahmed, H. I. Green synthesis and characterization of silver nanoparticles for reducing the damage to sperm parameters in diabetic compared to Metformin. *Sci. Rep.* **13**, 2256. https://doi.org/10.1038/s41598-023-29412-3 (2023).
38. Abo-El-Yazid, Z. H., Ahmed, O. K., El-Tholoth, M. & Ali, M. A. S. Green synthesized silver nanoparticles using *Cyperus rotundus* L. extract as a potential antiviral agent against infectious laryngotracheitis and infectious bronchitis viruses in chickens. *Chem. Biol. Technol. Agric.* **9**, 55. https://doi.org/10.1186/s40538-022-00325-z (2022).
39. Das, P., Ghosal, K., Jana, N. K., Mukherjee, A. & Basak, P. Green synthesis and characterization of silver nanoparticles using Belladonna mother tincture and its efficacy as a potential antibacterial and anti-inflammatory agent. *Mater. Chem. Phys.* **228**, 310–317. https://doi.org/10.1016/j.matchemphys.2019.02.064 (2019).
40. Ghosh, B. et al. Facile fabrication of Nishamalaki Churna mediated silver nanoparticles with antibacterial application. *Heliyon.* **9** https://doi.org/10.1016/j.heliyon.2023.e18788 (2023).
41. Izak-Nau, E. et al. Impact of storage conditions and storage time on silver nanoparticles' physicochemical properties and implications for their biological effects. *RSC Adv.* **5**, 84172–84185. https://doi.org/10.1039/C5RA10187E (2015).
42. Iravani, S. Green synthesis of metal nanoparticles using plants. *Green. Chem.* **13**, 2638–2650. https://doi.org/10.1039/C1GC15386B (2011).
43. Prabhakaran, M. P., Venugopal, J., Chan, C. K. & Ramakrishna, S. Surface modified electrospun nanofibrous scaffolds for nerve tissue engineering. *Nanotechnology.* **19**, 455102. https://doi.org/10.1088/0957-4484/19/45/455102 (2008).
44. Xu, F., Shi, Y. C. & Wang, D. X-ray scattering studies of lignocellulosic biomass: a review. *Carbohydr. Polym.* **94** (2), 904–917. https://doi.org/10.1016/j.carbpol.2013.02.008 (2013).
45. Ahmed, S., Ahmad, M., Swami, B. L. & Ikram, S. Green synthesis of silver nanoparticles using *Azadirachta indica* aqueous leaf extract. *J. Radiat. Res. Appl. Sci.* **9**, 1–7. https://doi.org/10.1016/j.jrras.2015.06.006 (2016).
46. Szymańska, E. et al. Multifunctional Tannic acid/silver nanoparticle-based mucoadhesive hydrogel for improved local treatment of HSV infection: in vitro and in vivo studies. *Int. J. Mol. Sci.* **19**, 387. https://doi.org/10.3390/ijms19020387 (2018).
47. Boateng, J. S., Matthews, K. H., Stevens, H. N. & Eccleston, G. M. Wound healing dressings and drug delivery systems: a review. *J. Pharm. Sci.* **97**, 2892–2923. https://doi.org/10.1002/jps.21210 (2008).
48. Haydee, B. F., Blanca, E. F., José, B. M. & Francisco-Javier, O. E. Use of β-Cyclodextrins to prevent modifications of the properties of carbopol hydrogels due to carbopol-Drug interactions. *Chem. Pharm. Bull.* **50**, 40–46 (2002).
49. More, P. R. et al. Silver nanoparticles: bactericidal and mechanistic approach against drug resistant pathogens. *Microorganisms.* **11** (369). https://doi.org/10.3390/microorganisms11020369 (2023).
50. Hu, M. et al. One-step construction of silver nanoparticles immersed hydrogels by triple-helix β-glucans and the application in infectious wound healing. *Int. J. Biol. Macromol.* **282**, 137146. https://doi.org/10.1016/j.ijbiomac.2024.137146 (2024).

51. Carvalho-Silva, J. M. & Dos Reis, A. C. Anti-inflammatory action of silver nanoparticles in vivo: systematic review and meta-analysis. *Heliyon*. https://doi.org/10.1016/j.heliyon.2024.e34564 (2024).
52. Hou, T. et al. Biomedical applications of chitosan-coated phytogenic silver nanoparticles: an alternative drug to foodborne pathogens. *Int. J. Biol. Macromol.* **280**, 135590. https://doi.org/10.1016/j.ijbiomac.2024.135590 (2024).
53. Verkhovskii, R. et al. Physical properties and cytotoxicity of silver nanoparticles under different polymeric stabilizers. *Heliyon*. **5** https://doi.org/10.1016/j.heliyon.2019.e01305 (2019).
54. Van De Vyver, M. et al. Histology scoring system for murine cutaneous wounds. *Stem Cells Dev.* **30**, 1141–1152 (2021).

Acknowledgements
The authors are grateful to the School of Pharmaceutical Sciences, Siksha O Anusandhan, Bhubaneswar, and NIPER, S.A.S. Nagar for providing the necessary facilities for carrying out this research work.

Author contributions
Su.S: Conceptualization, data curation, resources, investigation, writing, original draft; A.B.: Conceptualization, data curation, supervision, writing—review & editing; S.B.: Investigation; Sh. S.: Investigation; I.R.: Supervision, writing—review & editing.

Funding
Open access funding provided by Siksha 'O' Anusandhan (Deemed To Be University)

Declarations

Competing interests
The authors declare no competing interests.

Additional information
Correspondence and requests for materials should be addressed to A.B.

Reprints and permissions information is available at www.nature.com/reprints.

Publisher's note Springer Nature remains neutral with regard to jurisdictional claims in published maps and institutional affiliations.